CALCULATION OF THREE-DIMENSIONAL COMPRESSIBLE LAMINAR AND TURBULENT BOUNDARY FLOWS

THREE-DIMENSIONAL COMPRESSIBLE BOUNDARY LAYERS OF REACTING GASES OVER REALISTIC CONFIGURATIONS

By Robert M. Kendall, William S. Bonnett, Charles T. Nardo, and Michael J. Abbett
Aerotherm Division, Acurex Corporation

SUMMARY

A three-dimensional boundary-layer code has been developed for particular application to realistic hypersonic aircraft, but it is very general and can be applied to a wide variety of boundary-layer flows. Laminar, transitional, and fully turbulent flows of compressible, reacting gases can be efficiently calculated by use of the code. A body-oriented orthogonal coordinate system is used for the calculation and the user has complete freedom in specifying the coordinate system within the restrictions that one coordinate must be normal to the surface and the three coordinates must be mutually orthogonal.

The boundary-layer equations are discretized and integrated step by step. The integration is fully implicit in the streamwise direction, a condition that is especially important for realistic configurations since it enables one to calculate flows having cross-flow attachment and detachment lines off the pitch plane. The code is restricted to those flows which are adequately represented by the boundary-layer equations; the analysis must be extended to adequately describe flows in which cross-flow diffusion effects are important near cross-flow attachment lines. The numerical algorithm includes splined functions for dependent variables between nodes to minimize the number of nodes normal to the surface. This condition results in an extremely efficient solution procedure for reacting boundary layers. Finally, the code includes the capability to account for surface normal entropy gradient effects.

INTRODUCTION

The design of aircraft and aerospace vehicles requires consideration of the inviscid/viscous flow field over the vehicle. Historically, the aerothermal environment of such aircraft in realistic flight conditions has been predicted by synthesizing empirical

data from ground-level test facilities with simplified analyses to correlate the test results with the anticipated flight environment. This approach depends on the development of scaling laws between ground and flight conditions. As flight regimes are further extended in altitude and speed to those appropriate to space shuttle and hypersonic research aircraft, the range of applicability of scaling laws and correlations relating results from existing test facilities to flight conditions becomes more uncertain. The cost of constructing test facilities which will yield data of sufficient quality and range to duplicate realistic vehicles and trajectories is prohibitive.

Parallel with the increased flight range typified by spacecraft, space shuttle, and hypersonic research aircraft has been a rapid increase in the ability to obtain numerically exact solutions to the complete gas dynamic equations for the inviscid/viscous flow field about such configurations. Currently, under contract NAS 1-11525 (ref. 1), The National Aeronautics and Space Administration is supporting the development of a computer code which will obtain the inviscid flow field solution. To predict adequately the viscous drag and heat flux distributions, one must obtain the solution of the three-dimensional boundary-layer equations describing the viscous layer adjacent to the vehicle surface. In this paper recent efforts which have culminated in the development of a computer code for solving general three-dimensional laminar and turbulent chemically reacting boundary layers are summarized.

The numerical approach used is based on the results of two pilot codes for calculating three-dimensional boundary layers on pointed cones at angle of attack as well as broad experience in developing and applying boundary-layer codes in two dimensions. Key elements in the approach are:

(a) Splined functions to minimize nodes through the boundary-layer thickness

(b) Finite differences used for cross-flow derivatives

(c) Physical variables, simplifying analyses, and changes in turbulent transport properties model

(d) Fully implicit solution procedure; thereby the convenient calculation of flows having off-pitch-plane attachment and detachment lines is permitted

(e) Relative ease in incorporating a wide variety of turbulence models and boundary conditions, including entropy layer, specified surface temperature or heat flux, surface catalysis, mass addition, coupling with surface ablation calculations, etc.

(f) Very reasonable computing time

The result is a code which can accurately describe laminar boundary-layer profiles with 7 to 10 nodes and turbulent profiles with 12 to 15 nodes through the boundary layer. The number of nodes through the boundary layer is important for reacting boundary layers

because the time required to evaluate the chemical state dominates the time spent in matrix inversion for macroscopic quantities u, v, w, and T where T is the temperature. Hence, the time implication of the number of nodes is more serious than it would be for homogeneous boundary layers. Conventional implicit finite-difference approaches are less complicated analytically but require significantly more nodes in the plane normal to the wall boundary than do splined function procedures, simply because the latter relate not only the dependent variables but also their derivatives with the nodal variation of the independent variables.

Three-dimensional boundary layers exhibit certain physical and mathematical characteristics which have important implications on the selection of a numerical solution technique. Particularly important to this effort are physical and mathematical modeling in the vicinity of outflow and inflow lines, lines where the surface streamlines diverge or converge. The windward side pitch plane line of a pointed cone at incidence is an example of an outflow line, whereas the leeward side pitch plane meridian at small incidence typifies an inflow line. These lines are often found off the pitch plane on both the windward and leeward sides of configurations such as the space shuttle. They are important physically because they are often regions of local maximum or minimum heat flux rates. Mathematically, they are extremely important because of a numerical approach often taken in solving three-dimensional boundary-layer flows, namely, integrating with cross flow.

Consider the pointed cone at incidence. Because the flow direction is strictly away from the windward pitch plane (except right on the pitch plane), one expects and finds that by assuming small circumferential derivatives, the solution of the boundary layer in the pitch plane can be determined completely independent of the boundary-layer solution off the pitch plane.[1] Assume for the moment that one has the entire flow field solution (inviscid and boundary layer) at some axial station x_0 and wishes to advance to $x_1 = x_0 + \Delta x$ where the inviscid solution is known (Δx is the mesh point spacing). As noted above, the windward pitch plane solution can be obtained directly. Then, by recalling that the initial value problem is hyperbolic-like with respect to the circumferential coordinate and parabolic with respect to the surface normal, the boundary-layer solution can be obtained by marching around the cone from the windward to the leeward side.

In contradistinction is the class of fully implicit solution procedures in which the solution at $x_1 = x_0 + \Delta x$ is obtained simultaneously at all points. In the fully implicit procedure each point at x_1 is influenced by and influences every other point. The influ-

---

[1]Of course, one needs information about the behavior of the edge inviscid flow in the vicinity of the pitch plane and of the pressure, temperature, velocity components, etc. (that is, not only p_e, T_e, u_e, etc., but also $\partial p_e/\partial \phi$, etc.).

ence will be large or negligibly small according to the actual physical influences, provided that the numerical scheme is accurate.

The circumferential marching methods require that one integrate the system in the direction of positive cross-flow velocity in order to obey the laws of propagation of signals. Marching against the cross flow results in instability. On a cone at very small incidence this is no problem, for the cross flow is always from windward to leeward. At higher incidence the cross-flow inflow line moves off the leeward meridian, and it is necessary to march from both the windward and the leeward meridians toward the cross-flow inflow line. Furthermore, the marching methods can have stability limits on the streamwise integration step size, and the allowable step size decreases linearly with the meridional spacing. Fully implicit schemes usually have no such integration step size limit, the only limit being one of accuracy.

Having used the pointed cone problem to clarify the situation, consider now a realistic configuration such as the space shuttle. Typical outflow and inflow lines on the windward side are shown in sketch (a). Obviously, the solution along the pitch plane out-

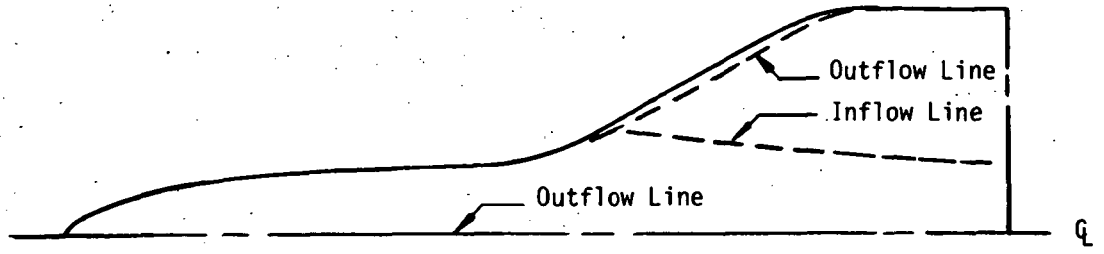

Sketch (a).- Schematic of inflow and outflow lines.

flow line can be obtained independently of the rest of the boundary layer by assuming small cross-flow derivatives. This is not the case for the wing leading edge because there are no symmetry conditions there which could be used to simplify the three-dimensional boundary-layer equations. In fact, without solving the complete problem, one does not know the locus of the outflow line there. Swept cylinder theory could be used to obtain an approximate solution along the wing leading edge, but this would be inconsistent with the spirit of an exact boundary-layer calculation. This is particularly important since the wing leading edge is a region of locally very high heat fluxes. The advantage of the fully implicit approach is apparent, for the exact solution including the wing leading-edge region can be obtained without resort to approximations.

There is another very important inflow line consideration. It is well known that there appear to be no physically meaningful similar solutions to the full three-dimensional boundary-layer equations on the leeside of a pointed cone at angle of attack α for values of α/θ_c in certain ranges. (See refs. 2 and 3.) (θ_c is the half-core angle.) One

expects comparable results to hold for inflow lines on realistic configurations. Lin and Rubin (ref. 3) suggest extending the three-dimensional boundary-layer equations to account for cross-flow diffusion, and they report results that show excellent agreement with experiment for values of α/θ_c for which they could not obtain numerical solutions on the leeside by using the standard three-dimensional boundary-layer equations. At even higher values of α/θ_c, however, they could obtain solutions with the three-dimensional boundary-layer equations (without cross-flow diffusion), but these solutions were in poor agreement with the experimental heat flux. Calculations using the extended equations agreed well with the experimental data.

ANALYSIS

Geometry and Coordinate Considerations

The selection of a coordinate system to describe the development of a boundary layer over a three-dimensional surface is of major importance and can significantly affect the eventual usefulness and applicability of the final computer code. The numerical algorithm utilized herein required the use of Taylor series spline functions (in the normal direction) and a Newton-Raphson iteration technique to obtain the final solution vectors. Both of these concepts are discussed in more detail later; however, it is useful to emphasize that such a solution procedure requires one to generate many correction coefficients for each individual term in the equation set. As a result, it becomes extremely desirable to keep the number of terms in the equation set to a minimum. Consequently, and because the flows to be computed will be generally highly nonsimilar, it was elected to retain both dependent and independent variables in their primitive forms (except for nodal-point stretching in the direction normal to the wall). Utilization of stream functions and similarity variables would result in significant increases in the number of terms in the equation set. In addition, such transformations can result in major difficulties as far as future code modifications and/or changes are concerned, especially in updating turbulence models.

The boundary-layer approximation is impractical to implement in any other than surface-oriented coordinate systems. Once this is recognized, the only remaining question is one of orthogonal compared with nonorthogonal coordinate systems. Regardless of which system is chosen, one constraint should be recognized, namely, that one coordinate direction must always be normal to the surface at all times. As a result, if one selects an orthogonal coordinate system, only one other coordinate direction is independent, as the third will automatically be determined from the orthogonality condition. For example, if the streamwise coordinate is selected (for example, to be coincident to the body cross sections), the nodal-point distribution in the circumferential direction is automatically determined. However, if the nodal point distribution in the circumferential

direction is specified, then constant streamwise coordinate stations will be, in general, skewed surfaces and will not lie along the body cross-section planes. On the other hand, if a nonorthogonal coordinate system is chosen, one may select both streamwise and circumferential nodal point distributions. To decide whether to stay orthogonal or nonorthogonal requires one to investigate the form of the equations in both instances. Consider the metric tensor g_{ij} in both coordinates:

For orthogonal systems:

$$g_{ij} = \begin{pmatrix} h_1^2 & 0 & 0 \\ 0 & h_2^2 & 0 \\ 0 & 0 & 1 \end{pmatrix}$$

For nonorthogonal systems:

$$g_{ij} = \begin{pmatrix} h_1^2 & h_1 h_2 \cos\theta & 0 \\ h_1 h_2 \cos\theta & h_2^2 & 0 \\ 0 & 0 & 1 \end{pmatrix}$$

where h_1 and h_2 are the scale factors.

The nonorthogonal metric tensor results in only two additional terms in the continuity equation beyond its orthogonal counterpart. In the momentum and energy equations, however, there is a threefold increase in the number of terms. By assuming that each term generates, on the average, three correction coefficients, one can easily assess that the nonorthogonal coordinate system results in a nominal tenfold increase in the number of correction coefficients.[2]

Although the desirability of choosing both surface coordinate point distributions is enticing, the additional complexity added to the analysis is not felt to be warranted. As a result, an orthogonal coordinate system was chosen. It was elected to have the flexibility of choosing a circumferential nodal-point distribution since it is necessary to be able to concentrate nodal points in regions of large cross-flow gradients (for example, wing leading edges). Since the other coordinate direction is normal to the wall, the third (streamwise) coordinate direction is automatically determined from the cross product. As a result, constant streamwise surfaces will not lie along body cross sections. This

[2]This result is only true if one considers cross-flow diffusion terms within the equation set. For no cross-flow diffusion, the increase is minimal. Although the equations presented herein do not include these additional terms, it is expected that their inclusion in the near future will be necessary in order to handle the cross-flow separation problem and for this reason the argument has been presented.

condition is inconvenient in that more handling and interpolation of edge conditions will be required to obtain a consistent set of edge boundary conditions.

It should be emphasized that the particular orthogonal system described is used in automatically coupling the boundary-layer code to the three-dimensional inviscid supersonic flow field code developed by Marconi et al. (ref. 1) for application to space shuttle problems. The boundary-layer code is written in general orthogonal surface coordinates, and one has the freedom to select any coordinate system within that class (for example, streamline coordinates), provided one can provide the inviscid edge data to the boundary-layer code.

Dependent and Independent Variable Selection

The governing equations are solved in primitive variables, but with stretching the independent variable normal to the surface for computational convenience. Transformations to similarity variables are useful in analytically studying similarity solutions. For the numerical solution of nonsimilar solutions their usefulness is of questionable value, provided nodal points are sensibly selected and streamwise derivatives are accurately represented. Cebeci et al. report (ref. 4) that fewer nodes were necessary for calculating turbulent boundary layers when they used a similarity transformation of the dependent variables, nodal spacing increasing geometrically from the wall. They would have had better results had they varied the nodal spacing logarithmically near the wall as the solution varies. Their experience simply indicates that geometrically spaced nodal distributions coupled with transformed dependent variables resulted in a nodal spacing which was closer to logarithmic in physical space than a straight geometric progression in physical space. To illustrate this condition, results of the 3-D code using physical variables and 8 nodes agrees very well with the BLIMP code (ref. 5) predictions using similarity variables and 7 nodes, as shown in figure 1. To minimize the number of points required, it is necessary to identify the edge of the boundary layer. This is done by scaling the lengths normal to the surface by the local boundary-layer thickness, an unknown quantity, which is obtained by introducing the auxiliary condition that the total enthalpy H_t at the second (or third) nodal point from the edge is a fixed ratio of the local edge enthalpy (for example, $H_t/H_{t,e} = 0.9$ at $x_3/x_{3,e} = 0.5$ where e denotes edge).

Governing Equations

The three-dimensional boundary-layer equations are written in general, orthogonal, body surface coordinates. One coordinate is normal to the local tangent plane, one is in the tangent plane in the general direction of the edge velocity,[3] and the third is in the tangent plane normal to the other two. As noted, coordinate stretching is performed normal to the surface. Within this context, the three-dimensional boundary-layer equations are

[3]This is necessary if the problem is to be solved as an initial value problem.

(subscript 1 indicates the general streamwise coordinate; subscript 2, the cross-flow coordinate; and subscript 3, the surface normal coordinate):

Continuity:

$$\frac{\partial}{\partial x_1}(h_2 \rho v_1) + \frac{\partial}{\partial x_2}(h_1 \rho v_2) + \frac{\partial}{\partial x_3}(h_1 h_2 \rho v_3) = 0 \tag{1}$$

Axial momentum:

$$\frac{v_1}{h_1}\frac{\partial v_1}{\partial x_1} + \frac{v_2}{h_2}\frac{\partial v_1}{\partial x_2} + v_3\frac{\partial v_1}{\partial x_3} + \frac{v_1 v_2}{h_1 h_2}\left(\frac{\partial h_1}{\partial x_2}\right) - \frac{v_2^2}{h_1 h_2}\left(\frac{\partial h_2}{\partial x_1}\right) = -\frac{1}{\rho h_1}\frac{\partial p}{\partial x_1} + \frac{1}{\rho}\frac{\partial}{\partial x_3}\left[(\mu + \epsilon)\frac{\partial v_1}{\partial x_3}\right]\frac{1}{Re} \tag{2}$$

Cross-flow momentum:

$$\frac{v_1}{h_1}\frac{\partial v_2}{\partial x_1} + \frac{v_2}{h_2}\frac{\partial v_2}{\partial x_2} + v_3\frac{\partial v_2}{\partial x_2} + \frac{v_1 v_2}{h_1 h_2}\left(\frac{\partial h_2}{\partial x_1}\right) - \frac{v_1^2}{h_1 h_2}\left(\frac{\partial h_1}{\partial x_2}\right) = -\frac{1}{\rho h_2}\frac{\partial p}{\partial x_2} + \frac{1}{\rho}\frac{\partial}{\partial x_3}\left[(\mu + \epsilon)\frac{\partial v_2}{\partial x_3}\right]\frac{1}{Re} \tag{3}$$

Normal momentum:

$$0 = -\frac{1}{\rho}\frac{\partial p}{\partial x_3} \tag{4}$$

Energy:

$$\rho\left(\frac{v_1}{h_1}\frac{\partial H}{\partial x_1} + \frac{v_2}{h_2}\frac{\partial H}{\partial x_2} + v_3\frac{\partial H}{\partial x_3}\right) = \frac{1}{Re}\frac{\partial}{\partial x_3}\left(B\left\{\epsilon - \frac{\epsilon}{2}\left[\frac{\hat{C}_p}{N_{Pr,t}} + \frac{1}{N_{Sc,t}}\left(\sum_i \frac{\partial K_i}{\partial h} h_i\right)\right] + \mu - \frac{\lambda_m}{2}\right\}\frac{\partial}{\partial x_3}\left(v_1^2 + v_2^2\right) + \left\{\epsilon\left[\frac{\hat{C}_p}{N_{Pr,t}} + \frac{1}{N_{Sc,t}}\left(\sum_i \frac{\partial K_i}{\partial h} h_i\right)\right] + \lambda_m\right\}\frac{\partial H}{\partial x_3}\right) \tag{5}$$

where p is the pressure, μ is the molecular viscosity, and

$$\lambda_m = \frac{1}{\mu_{ref}}\left[\lambda\frac{\partial T}{\partial h} - \sum_i j_i h_i\left(\frac{dh}{dx_3}\right)^{-1}\right]$$

$$\hat{C}_p = C_p\frac{\partial T}{\partial h}$$

and ϵ is the eddy viscosity. These equations are nondimensionalized, all dimensional quantities being divided by appropriate constant reference quantities. Important nondimensional groups are listed in table I.

TABLE I.- IMPORTANT NONDIMENSIONAL GROUPS

Group symbol	Elements	Common name
R_e, R, R_N, R_∞, $R_{e,\infty}$ $= \frac{\rho u \ell}{\mu}$	ρ reference density u reference velocity ℓ reference length μ reference viscosity	Reference Reynolds number Reynolds number based on nose radius Free-stream Reynolds number Reference free-stream Reynolds number
$B = \frac{u^2}{h}$	u reference velocity h reference enthalpy	
$N_{Pr,t} = \frac{C_p \epsilon}{\lambda}$	C_p specific heat ϵ eddy viscosity λ thermal conductivity	Turbulent Prandtl number
$N_{Sc,t} = \frac{\epsilon}{\rho D_{12}}$	ϵ eddy viscosity ρ density D_{12} binary diffusion coefficient	Turbulent Schmidt number

Numerical Procedures

To simplify the discussion, consider a three-dimensional Cartesian coordinate system x,y,z with velocity components u, v, and w. The x-coordinate corresponds to the direction of integration, y is locally normal to the surface, and z designates the cross-flow direction. The solution domain is covered by a nodal network as schematized in figure 2. It is assumed that the entire flow is known at some value $x = x_i$ and is to be determined at $x_{i+1} = x_i + \Delta x$. For a solution at x_{i+1} to be obtained, which satisfies the governing partial differential equations (PDEs) and the imposed boundary conditions, the functional form of the x, y, and z derivatives is specified and is substituted into the PDEs along with the boundary conditions. The result is a system of algebraic relations between unknown dependent variables at the nodal points at station $x = x_{i+1}$. Essentially all numerical solutions to the PDEs reduce to this same process. What distinguishes one procedure from another is the functional form chosen to relate nodal values of dependent variables and their derivatives, one to another.

Normal to the wall boundary, the dependent variables are represented by a splined Taylor series between each node. Letting j denote a nodal index running from 1 at the wall to JMAX at the outer edge of the boundary layer results in

$$\left.\begin{aligned} u_{j+1} &= u_j + u'_j\,\Delta y + u''_j\,\frac{\Delta y^2}{2} \\ u'_{j+1} &= u'_j + u''_j\,\Delta y \end{aligned}\right\} \tag{6}$$

In addition, the PDEs are integrated with respect to y between each node which insures that the conservation laws are satisfied exactly between nodes and greatly simplifies the calculation of diffusion terms by eliminating second derivatives.

In the cross-flow direction where variations are generally much less severe than in the normal direction, second-order-accurate centered finite differences are used to represent the cross-flow derivatives; for example, $\partial U/\partial z$ for equal spacing is represented as

$$U_Z = \frac{U_{j,k+1} - U_{j,k-1}}{z_{k+1} - z_{k-1}} \tag{7}$$

where k is the index associated with the z coordinate.

Axial derivatives $\partial U/\partial x$ are represented by simple backward difference quotients of the form

$$U_X = \frac{U_{i+1,j,k} - U_{i,j,k}}{x_{i+1} - x_i} \tag{8}$$

where i is the index associated with the x coordinate.

The solution is obtained fully implicitly. Thus, equations (6) and (7) are evaluated at station x_{i+1}. Upon introduction of the boundary conditions (for example, $U_{i+i,JMAX,k} = U_e(x,y,z)$, etc.), the result is a system of nonlinear algebraic equations for primary (u, ρ, etc.) and secondary (u', ρ', etc.) variables at each nodal point.[4] This system is solved by Newton-Raphson iteration as outlined in the following paragraph.

Consider the system of nonlinear equations to be represented by

$$F_m(U_n) = 0 \tag{9}$$

where m is an equation index and U_n is one of the dependent primary or secondary variables ($U_{i+1,j,k}$, etc.). Assume a value of $U_n = U_n^*$ and expand F_m (see eq. (9)) in a Taylor series about U_n^*

[4]Actually, obtaining the solution is usually enhanced if the derivative terms (u', ρ', etc.) are treated as the primary variables and the primitive variables (u, ρ, etc.) as the secondary variables.

$$F_m(U_n) = F_m(U_n^*) + \sum_{\ell} (U_\ell - U_\ell^*) \frac{\partial F_m}{\partial (U_\ell)_{U_\ell = U^*}} = 0 \tag{10}$$

This equation can be written in matrix form as

$$A(U - U^*) + F = 0 \tag{11}$$

or

$$U = U^* - A^{-1}F \tag{12}$$

where

$$A^{-1} = \left[\frac{\partial F_m}{\partial U_\ell}\right]^{-1} \tag{13}$$

Thus, the solution basically reduces to the problem of inverting a large matrix, and thereby solving a system of linear algebraic equations for the unknown U.

The matrix A is composed of a number of submatrices, illustrated in figure 3 for the case of five meridional (cross-flow) planes. It is block tridiagonal because cross-flow derivatives are represented with centered finite differences (if splined polynomials were used in the cross-flow direction as well, A would be dense matrix). The submatrices along the diagonal are relatively dense because they include information which is transmitted through the boundary layer as well as that which is transmitted in the cross-flow direction. The off-diagonal submatrices are relatively sparse because they only contain cross-flow derivative information.

A schematic of a typical diagonal submatrix for one meridional plane is shown in figure 4. Denote the submatrices by A_{ij} and decompose the unknown vector U into subvectors U_i. For a given value of U denote the error in the equation by E, which is a vector which can be similarly decomposed into subvectors E_i. Then the elements of the submatrix A_{ij}, which are denoted by a_{mn}, represent the rate of change of the mth equation at that node with respect to the nth dependent variable. The equations being considered are the Taylor series equations used in the spline fits of dependent variables, the governing PDEs, and certain constraint equations used in imposing boundary conditions.[5] Since the form of the Taylor series is invariant from node to node and station to station, the corresponding elements are constant. By taking advantage of this constancy, the submatrix can be further reduced as follows.[6]

---

[5]For example, $H/H_{te} = 0.9$ at $y/y_e = 0.5$. Additional constraints are appropriate for calculations involving vortical-layer effects.

[6]Do not confuse the sub submatrix A above with the complete matrix A of figure 3 and equation (11).

$$\begin{matrix}\uparrow \\ \text{Taylor} \\ \text{series} \\ \downarrow\end{matrix} \quad \overset{\text{Submatrix reduction}}{\begin{bmatrix} A & B \\ C & D \end{bmatrix} \begin{bmatrix} U_1 \\ U_2 \end{bmatrix} = \begin{bmatrix} 0 \\ E_2 \end{bmatrix}} \tag{14}$$

or

$$U_2 = \left(D - CA^{-1}B\right)^{-1} E_2 \tag{15}$$

and

$$U_1 = A^{-1}BU_2 \tag{16}$$

Return now to the complete system equations (9). Since A is block tridiagonal, it can be reduced by Gaussian reduction. In this reduction, it is necessary to invert a number of submatrices. Because of the properties of the submatrices (see discussion of eqs. (14) to (16)), it is only necessary to invert matrices whose size is

$$\underset{\substack{\uparrow \\ \text{Equations} \\ \text{per node}}}{4} \times (\text{Number of nodes}) + \underset{\substack{\uparrow \\ \text{Constraint} \\ \text{equations}}}{3} \tag{17}$$

Thus, even though the complete matrix A is very large, the maximum matrix size which must be inverted is quite manageable, being typically about 35×35 for laminar flow and 63×63 for turbulent flow.

Stagnation-Point Solution

It is assumed that the flow is similar at the stagnation point. By placing the coordinate system origin at the stagnation point and orienting it near the stagnation point, the edge velocities can be expressed in the form[7]

$$\left.\begin{aligned} U_e &= U\frac{x}{\ell} \\ W_e &= W\frac{z}{\ell} \end{aligned}\right\} \tag{18}$$

where U and W are constants supplied by the inviscid solution. In the vicinity of the stagnation point

$$\left.\begin{aligned} \frac{du}{dx_1} &= \frac{u}{x_1} \\ \frac{dw}{dx_1} &= \frac{w}{x_1} \end{aligned}\right\} \tag{19}$$

[7]These expressions are for Cartesian coordinates.

and it is noted that

$$\frac{dg}{dx_1} = 0 \tag{20}$$

where g is the static enthalpy. In polar coordinates,

$$U_e = U \cos^2 \phi + W \sin^2 \phi \frac{x_1}{\ell} \tag{21}$$

$$W_e = (W - U)\cos \phi \sin \phi \frac{x_1}{\ell} \tag{22}$$

Since the cross-flow derivatives are well behaved at the stagnation point, the stagnation-point solution can be numerically generated by representing the streamwise derivatives as

$$\frac{du}{dx_1} = d_1 U_\ell - d_2 U_{\ell-1} \tag{23}$$

where

$$d_1 = -d_2 = \frac{1}{\Delta x_i} \tag{24}$$

By taking

$$\left.\begin{aligned} d_1 &= \frac{1}{x_e} \\ d_2 &= 0 \end{aligned}\right\} \tag{25}$$

for $\frac{du}{dx_1}$ and $\frac{dw}{dx_1}$ and $d_1 = d_2 = 0$ for $\frac{dg}{dx_1}$, the solution can be numerically generated very near the stagnation point. The predicted velocity profiles for the stagnation-point flow on a 4:1 prolate spheroid are compared with Howarth's analytical solution (ref. 6) in figure 5.

Entropy-Layer Effects

It is usually relatively simple to account for entropy-layer effects in two-dimensional or axisymmetric hypersonic flow over a blunt body. The usual procedure is to relate the mass flux in the boundary layer with the position on the bow shock wave encompassing the same amount of mass flux, as illustrated in sketch (b). That is, y_s is determined so that the mass flux between AA' equals that across the boundary layer BB'. The local edge conditions at B are then determined by isentropically expanding the streamline from behind the shock at A to the local surface pressure at B'. It is relatively easy to account for the effects of normal entropy gradient as well. Naturally,

the solution at BB' must be obtained iteratively in order to simultaneously satisfy the mass balance as indicated.

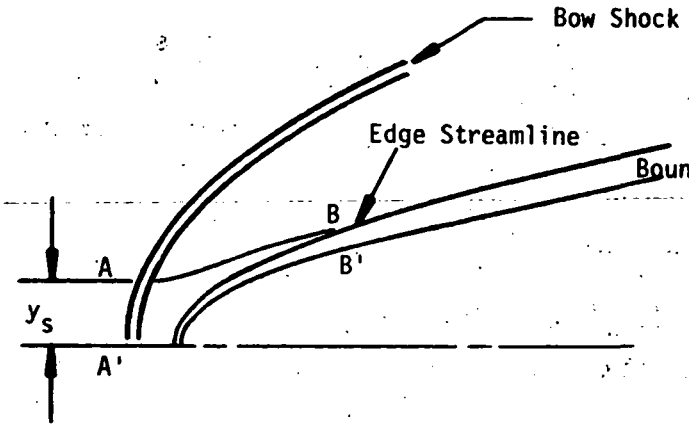

Sketch (b).- Schematic of 2-D or axisymmetric mass flux balance used in accounting for entropy layer effects.

In three dimensions the problem is somewhat more complicated, but not tremendously so. Again, for ease of exposition, revert to simple Cartesian coordinates. The idea is to match the viscous and inviscid solutions in some common region of overlap. To this end, define a stream surface S in the inviscid region, where the boundary-layer equations are still valid. Conservation of mass gives

$$\left.\begin{aligned} \frac{\partial F_x{}^i}{\partial x} + \frac{\partial F_z{}^i}{\partial z} &= 0 \\ \frac{\partial F_x}{\partial x} + \frac{\partial F_z}{\partial z} &= (\rho v)_{wall} \end{aligned}\right\} \tag{26}$$

where

$$\left.\begin{aligned} F_x{}^i &= \int_0^S (\rho u)^i dy \\ F_x &= \int_0^S (\rho u) dy \\ &\vdots \end{aligned}\right\} \tag{27}$$

Define

$$\left.\begin{aligned} \Delta F_x &= F_x - F_x{}^i \\ \Delta F_z &= F_z - F_z{}^i \end{aligned}\right\} \tag{28}$$

then

$$\frac{\partial \Delta F_x}{\partial x} + \frac{\partial \Delta F_z}{\partial z} = (\rho v)_{wall} \tag{29}$$

Note that $F - F^i = \text{Constant}$ outside the boundary layer (that is, in the overlap region). Thus ΔF_x and ΔF_z are independent of the location of S and are functions of x and z only so long as S is chosen to be in the overlap region. Equation (29) and one of equations (28) are the relations necessary to account for entropy-layer effects in three dimensions. They are implemented in the code as follows.

From the inviscid solution the values of the ΔF_x and ΔF_z functions at each (x,z) location are determined; next, the edge conditions are determined as functions of ΔF_x and ΔF_z, namely

$$U_e = f_1\left(x,z,F_x{}^i = F_x + \Delta F_x\right) \tag{30}$$

$$F_z{}^i = f_2\left(x,z,F_x{}^i = F_x + \Delta F_x\right) \tag{31}$$

etc. The two new equations at each meridional plane are introduced

$$\frac{\partial \Delta F_x}{\partial x} + \frac{\partial \Delta F_z}{\partial z} = (\rho v)_{wall} \tag{32}$$

$$\Delta F_z = F_z - F_z{}^i = F_z - f_2(x,z,F_x,\Delta F_x) \tag{33}$$

where F_x and F_z are available within the existing B/L solution logic. Equations (27) and (30) are the two constraint equations associated with entropy-layer effects previously discussed.

Turbulence Modeling

Mean field turbulence models are utilized in the present paper. The turbulent eddy viscosity model currently implemented in the code is the Bushnell-Beckwith model (ref. 7) as extended to three-dimensional flows by Harris. The eddy viscosity is given by

$$\epsilon = \rho \ell^2 \sqrt{\left(\frac{\partial u}{\partial x}\right)^2 + \left(\frac{\partial w}{\partial z}\right)^2} \tag{34}$$

where

$$\left.\frac{\ell}{\delta}\right|_{\frac{u}{u_e}=0.995} = K_1 \tanh\left(\frac{K_2}{K_1}\frac{y}{\delta}\right) D\bar{\gamma} \tag{35}$$

and

D wall damping function

$\overline{\gamma}$ y-direction intermittency function

In the transition region, ϵ is multiplied by a streamwise intermittency function. The turbulent Lewis and Prandtl numbers are taken to be constant.

Introduction of different turbulent eddy viscosity models is a straightforward task, but it does require the derivation of certain terms needed in the Newton-Raphson iteration (for example, $\partial\epsilon/\partial\rho$, $\partial\epsilon/\partial u$, etc.).

Thermochemistry

The code has ideal gas and chemical equilibrium options. In the latter case, the state relation is obtained by solving exactly for the species equilibrium relations in a special, optimized air equilibrium routine. Details are given in reference 5. It is a straightforward matter to replace the air equilibrium routine with a Mollier fit, if desired.

PRELIMINARY RESULTS

A number of test cases are currently in progress. In this section the results of predictions are compared with experimental heat-transfer data for two three-dimensional flows.

The first is for a laminar boundary layer on a 10° half-angle cone at an angle of attack of 4°. The experimental data were obtained by Tracy (ref. 8) at $M_\infty = 7.95$ and $R_{e,\infty} = 1.25 \times 10^6$ per foot. The inviscid edge data for the boundary-layer calculation were obtained from Jones' tables (ref. 9). The predicted circumferential distribution of heat-transfer coefficient is compared with the experimental data in figure 6, where it is seen that the agreement is excellent.

The second sample problem is for laminar flow over a 2.79-cm (1.1-in.) R_N sphere/15° cone at an angle of attack of 10°. The tests were conducted at free-stream Mach and Reynolds numbers of 10.6 and 4.1×10^6 per meter (1.2×10^6 per foot) (Cleary, ref. 10). Theoretical heat-transfer distributions are compared with experimental data in figures 7 and 8. Axial distributions along different meridional rays are given in figure 7 and the circumferential distribution at one fixed axial station is given in figure 8. The theoretical calculations were generated by using normal-shock entropy. In general, the agreement between theory and experiment is very good. Slightly higher predictions

on the windward side at $x/R_N < 2$ probably result from a rather large axial step size and the resulting inaccuracies in numerically calculating the local edge pressure gradient.

CONCLUDING REMARKS

The three-dimensional boundary-layer code reported herein has been developed for particular application to realistic hypersonic aircraft, but it is very general and can be applied to a wide variety of boundary-layer flows of interest. Laminar, transitional, and fully turbulent flows of compressible, reacting gases can be efficiently calculated by use of the code. The calculation is performed in a general body-oriented orthogonal coordinate system. The user has complete freedom in specifying the coordinate system within the restrictions that one coordinate must be normal to the surface and the three coordinates must be mutually orthogonal.

The boundary-layer equations are discretized and integrated step by step. The integration is fully implicit in the streamwise direction. This is especially important for realistic configurations since it enables one to calculate flows having cross-flow attachment and detachment lines off the pitch plane. The code is restricted to those flows which are adequately represented by the boundary-layer equations; the analysis must be extended to describe adequately flows in which cross-flow diffusion effects are important near cross-flow attachment lines. The numerical algorithm includes splined functions for dependent variables between nodes to minimize the number of nodes normal to the surface. This condition results in an extremely efficient solution procedure for reacting boundary layers. Finally, the code includes the capability to account for surface normal entropy gradient effects.

Currently, the code is being coupled to the supersonic, inviscid flow field code which was developed by Marconi et. al., Grumman Aerospace Corporation, under contract to the National Aeronautics and Space Administration. Upon completion of the inviscid/viscid code coupling, extensive comparisons for more complex configurations will be made.

REFERENCES

1. Marconi, Frank; Yaeger, Larry; and Hamilton, H. Harris: Computation of High-Speed Inviscid Flows About Real Configurations. Aerodynamic Analyses Requiring Advanced Computers, Part II, NASA SP-347, 1975, pp. 1411-1455.

2. Murdock, John W.: The Solution of Sharp Cone Boundary Layer Equations in the Plane-of-Symmetry. SAMBO TR-71-209, U.S. Air Force, July 1971. (Available from DDC as AD 730 598.)

3. Lin, T. C.; and Rubin, S. G.: Viscous Flow Over a Cone at Moderate Incidence. II. - Supersonic Boundary Layer. AFOSR-TR-73-0219, U.S. Air Force, Sept. 1972. (Available from DDC as AD 755 862.)

4. Cebeci, Tuncer; Kaups, Kalle; Mosinskis, G. J.; and Rehn, J. A.: Some Problems of the Calculation of Three-Dimensional Boundary-Layer Flows on General Configurations. NASA CR-2285, 1973.

5. Kendall, Robert M.: An Analysis of the Coupled Chemically Reacting Boundary Layer and Charring Ablator. Pt. V – A General Approach to the Thermochemical Solution of Mixed Equilibrium-Nonequilibrium, Homogeneous or Heterogeneous Systems. NASA CR-1064, 1968.

6. Rosenhead, L., ed.: Laminar Boundary Layers. Clarendon Press (Oxford), 1963.

7. Bushnell, Dennis M.; and Beckwith, Ivan E.: Calculation of Nonequilibrium Hypersonic Turbulent Boundary Layers and Comparisons With Experimental Data. AIAA J., vol. 8, no. 8, Aug. 1970, pp. 1462-1469.

8. Tracy, Richard R.: Hypersonic Flow over a Yawed Circular Cone. Hypersonic Res. Proj. Mem. No. 69 (Contract No. DA-31-124-ARO(D)-33), Graduate Aeronaut. Lab., California Inst. Technol., Aug. 1, 1963.

9. Jones, D. J.: Tables of Inviscid Supersonic Flow About Circular Cones at Incidence $\gamma = 1.4$. AGARDograph 137, Pts. I and II, Nov. 1969.

10. Cleary, Joseph W.: Effects of Angle of Attack and Bluntness on Laminar Heating-Rate Distributions of a 15° Cone at a Mach Number of 10.6. NASA TN D-5450, 1969.

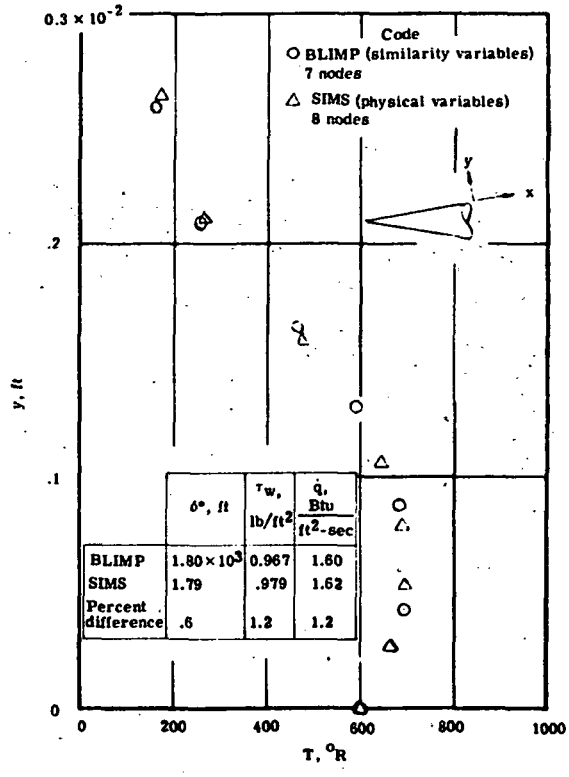

Figure 1.- Illustration that physical variables require no more nodes than transformed variables. Laminar flow; $M_\infty = 8$; $\gamma = 1.4$; $R_\infty = 8.5 \times 10^6$; $\theta_c = 10^o$; $\alpha = 0^o$; γ, ratio of specific heat; τ_w, shear stress at wall; δ^*, displacement thickness; and q, heat transfer.

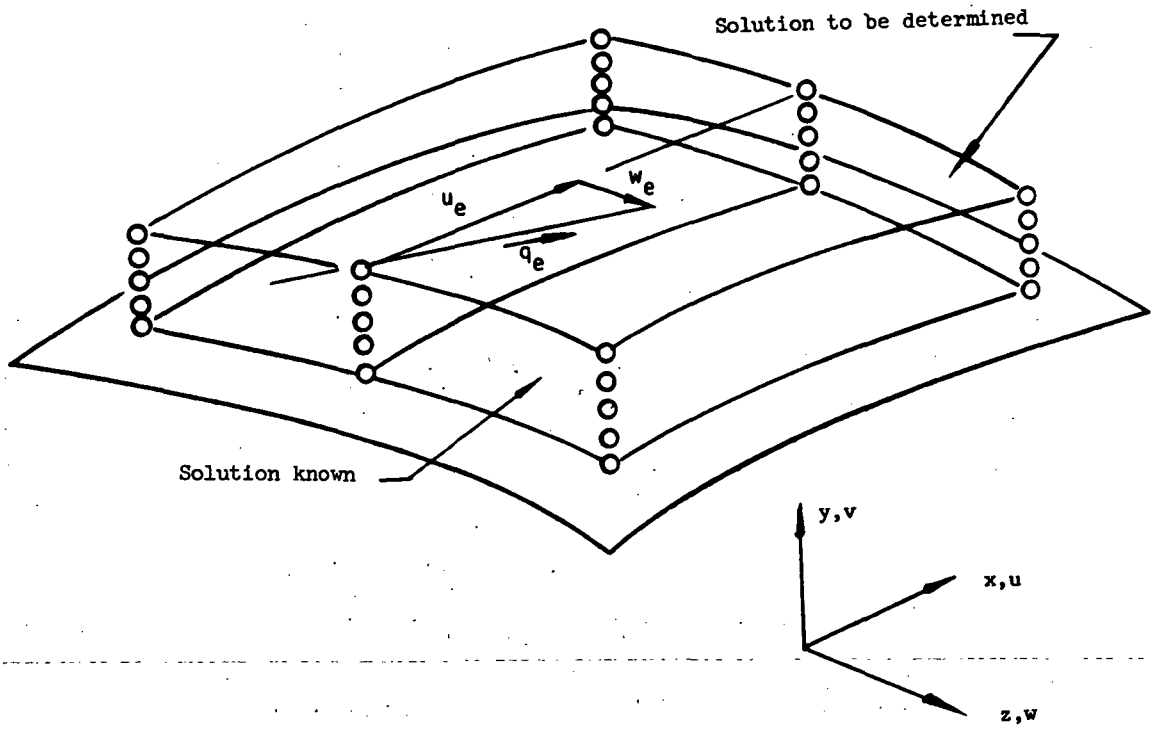

Figure 2.- Schematic of discretization. Boundary layer is covered by a nodal network.

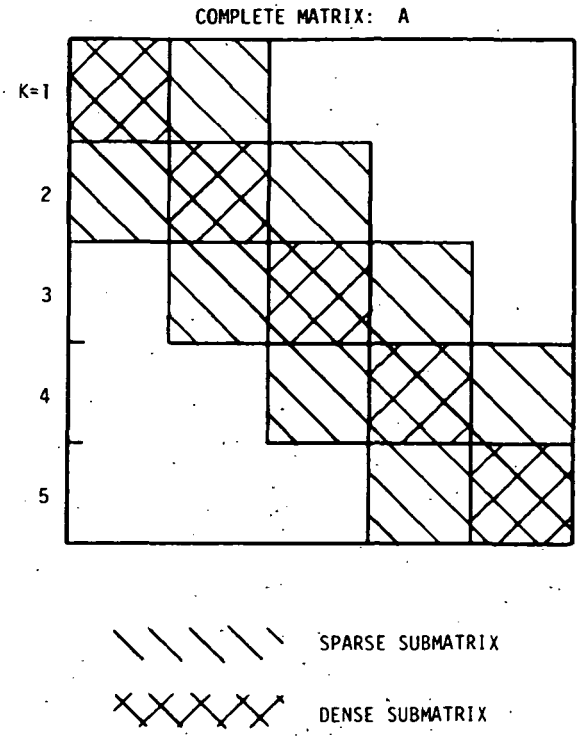

Figure 3.- Schematic of form of matrix A for the case of five meridional planes.

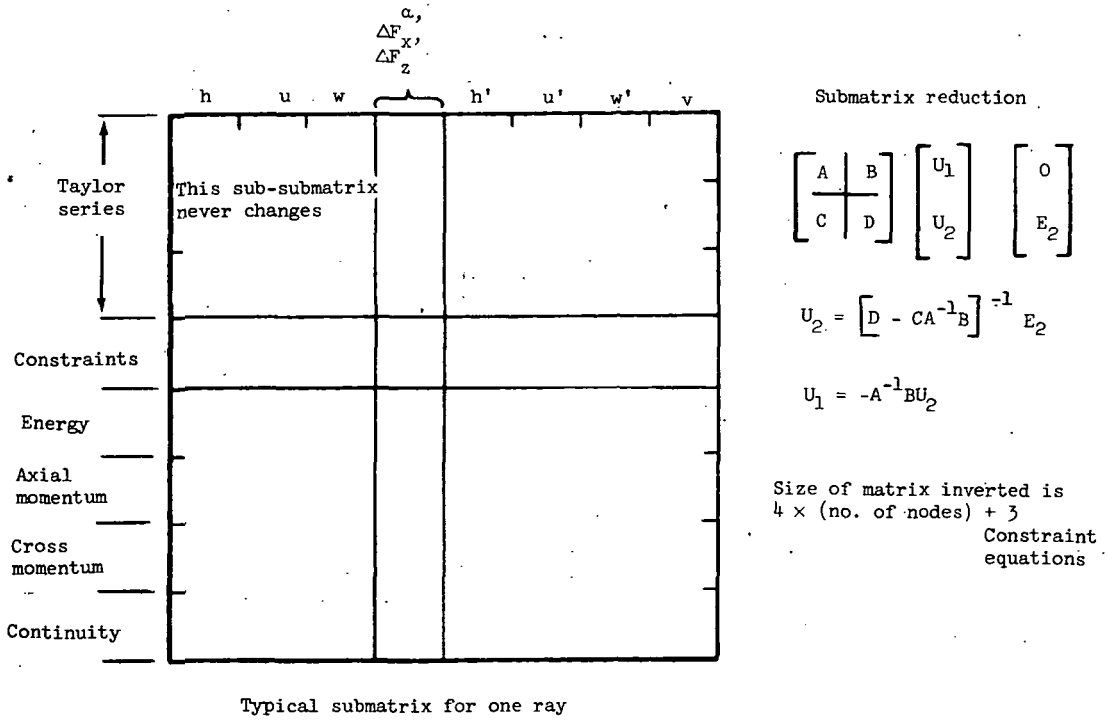

Figure 4.- Schematic of submatrix.

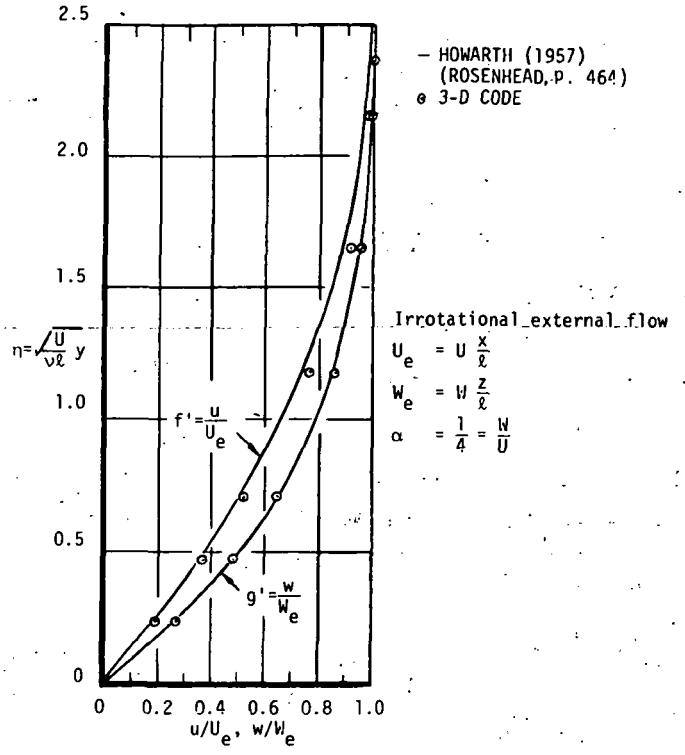

Figure 5.- Comparison of exact and approximate general 3-D stagnation-point solution. ν is kinematic viscosity.

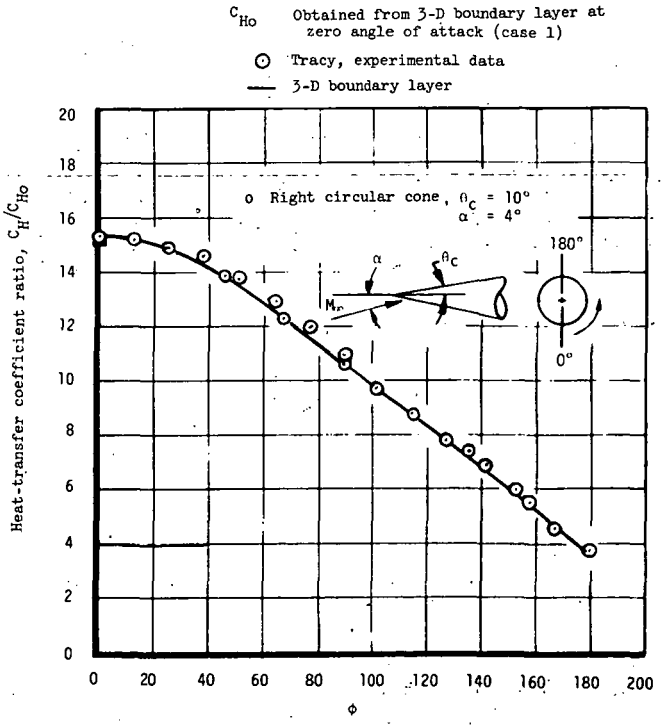

Figure 6.- Comparison of 3-D boundary-layer solution to experimental data.

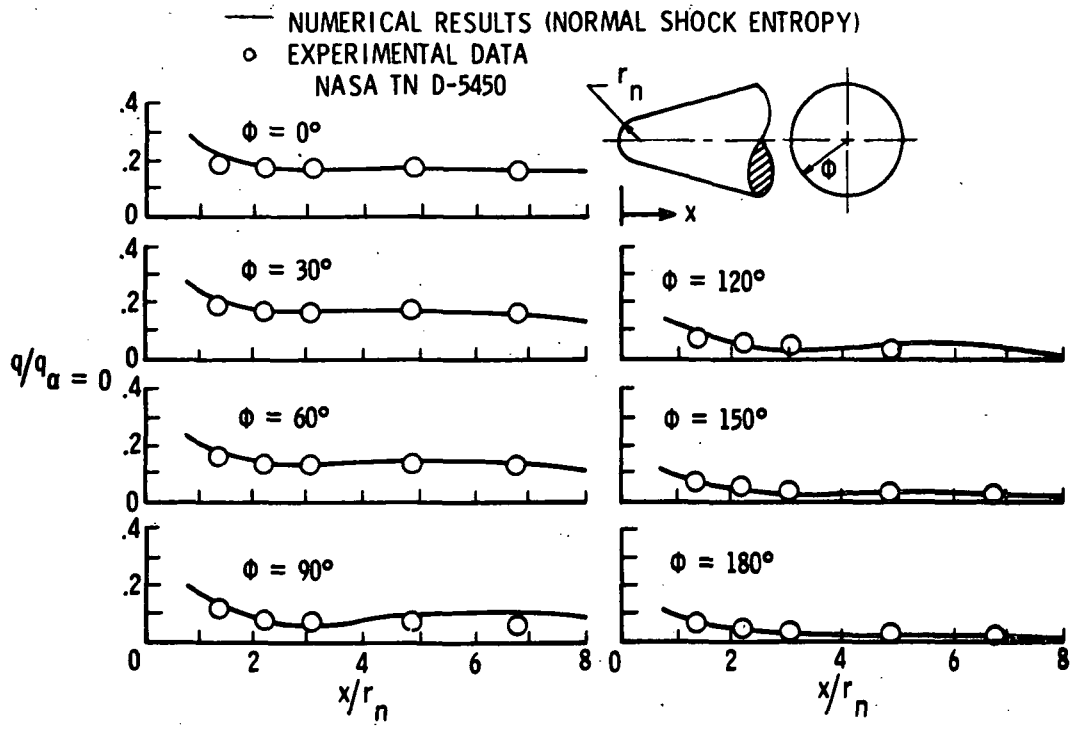

Figure 7.- Comparison of numerical results with experimental data. Axial heat-transfer distributions for 15° cone; $M_\infty = 10.6$; $R_\infty = 1.2 \times 10^6$; and $\alpha = 10°$.

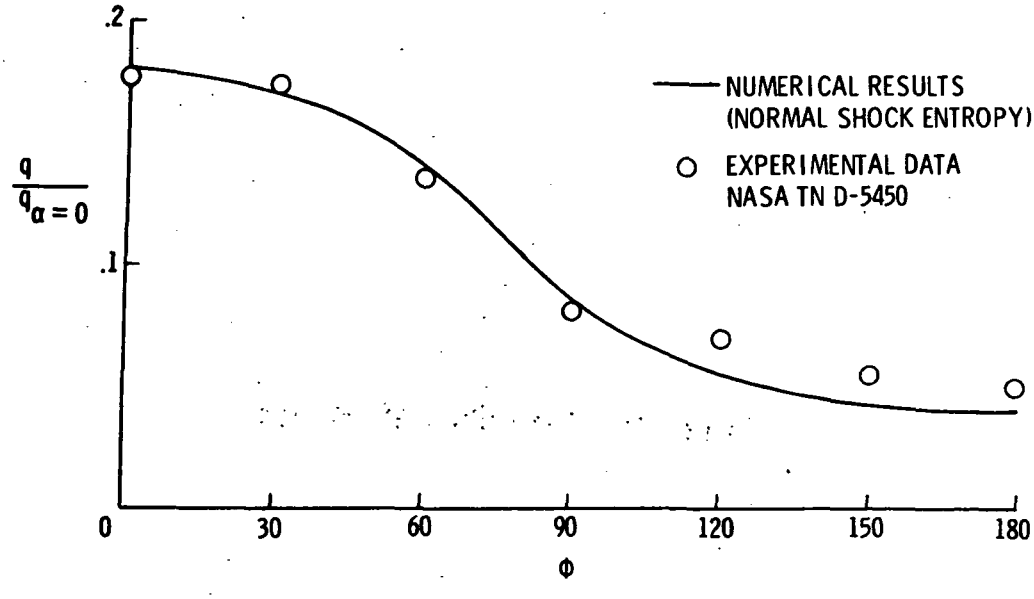

Figure 8.- Comparison of numerical results with experimental data. Circumferential heat-transfer distribution. $M_\infty = 10.6$; $R_\infty = 1.2 \times 10^6$; $\alpha = 10°$; and $x/r_n = 2.23$.